
White Rose Research Online

eprints@whiterose.ac.uk
https://eprints.whiterose.ac.uk
Universities of Leeds, Sheffield and York

Deposited via The University of Sheffield.

White Rose Research Online URL for this paper:
https://eprints.whiterose.ac.uk/id/eprint/146745/

Version: Accepted Version

Article:
Li, Y., Zhu, Z.Q., Wu, X. et al. (2019) Comparative study of modular dual 3-phase permanent magnet machines with overlapping/non-overlapping windings. IEEE Transactions on Industry Applications, 55 (4). pp. 3566-3576. ISSN: 0093-9994

https://doi.org/10.1109/tia.2019.2908138

© 2019 IEEE. Personal use of this material is permitted. Permission from IEEE must be obtained for all other users, including reprinting/ republishing this material for advertising or promotional purposes, creating new collective works for resale or redistribution to servers or lists, or reuse of any copyrighted components of this work in other works. Reproduced in accordance with the publisher's self-archiving policy.

Reuse
Items deposited in White Rose Research Online are protected by copyright, with all rights reserved unless indicated otherwise. They may be downloaded and/or printed for private study, or other acts as permitted by national copyright laws. The publisher or other rights holders may allow further reproduction and re-use of the full text version. This is indicated by the licence information on the White Rose Research Online record for the item.

Takedown
If you consider content in White Rose Research Online to be in breach of UK law, please notify us by emailing eprints@whiterose.ac.uk including the URL of the record and the reason for the withdrawal request.

UNIVERSITY OF LEEDS

University of Sheffield

UNIVERSITY of York

Comparative Study of Modular Dual 3-phase Permanent Magnet Machines with Overlapping/Non-overlapping Windings

Y. X. Li, Z. Q. Zhu, *Fellow, IEEE*, X. M. Wu, A. S. Thomas, and Z. Y. Wu

***Abstract*—For modular permanent magnet (PM) machines with overlapping (OLP) windings widely employed in wind power generation, the large torque ripple and long end winding are major issues. In order to solve these problems, PM machines with non-overlapping (NOLP) windings and redundant teeth for easy modularity are proposed in this paper. The comparative study between modular machines with these two kinds of windings is necessary and the major focus of this paper. For the sake of clarity, two modular dual 3-phase machines with 42-slots/32-poles (42S/32P) and 192S/32P combinations are chosen as examples to show the differences in terms of the machine performance. The proposed 42S/32P modular machine adopts NOLP winding, while the conventional 192S/32P one uses OLP type. Based on the results, it is found that the modular machine with NOLP winding has comparable average torque and efficiency. In the meantime, much lower torque ripple exists for the proposed modular machine regardless of the current value. The shorter and simpler end windings are beneficial to manufacturability. Moreover, the proposed modular machine with NOLP winding will be more fault-tolerant due to smaller mutual inductances between phases and larger *d*-axis inductance. Finally, the proposed 42S/32P modular machine is prototyped and the experiments validate the correctness of the analyses in this paper. Despite two specific examples being used, the conclusion should be generic and can be employed to modular machines with other slot and pole number combinations.**

***Index Terms*— Dual 3-phase machine, modular machine, non-overlapping winding, overlapping winding, permanent magnet machine.**

I. Introduction

With the development of power converter techniques and higher requirement for system reliability, multi-phase electrical machines have become the research hot spot in recent years [1]. The advantages of adopting multi-phase electrical machines include low power rating of each phase, high redundancy of the electrical machine system and decent torque performance, etc. Besides, the fault-tolerant capability is good as well [2].

Among all of the multi-phase electrical machines, those adopting dual 3-phase integer slot overlapping (OLP) windings have gained increasing attention over the past few decades [3]-[11]. Authors in [3] tried to build up the dual 3-phase electrical machine models with any displaced angle between two sets of windings. However, the mutual coupling was still not fully avoided. The redundancy of multi-phase electrical machines with independent inverter supplied has been addressed in [4] where dual 3-phase electrical machines being used as the example. The definition of phase number was clarified in [5] and the merit of dual 3-phase winding that more harmonics are eliminated compared with single 3-phase winding can be clearly seen. The detailed analysis of induction motors with dual 3-phase windings in [6] further shows the advantage of loss reduction for this kind of winding. When dual 3-phase windings are used, there will be more space voltage vectors being selected to improve the torque performance [7]. To more easily employ the space vector pulse width modulation (SVPWM) technique, a decoupled orthogonal transformation was developed in [8]. More design details about dual 3-phase electrical machines and the application of SVPWM technique to reduce torque ripple were investigated in [9] and [10]. The comparison between dual 3-phase electrical machines with thirty and zero degree phase shift between two sets of windings (named as “Thirty Type” and “Zero Type”) was executed in [11] from a variety of aspects. Each type has its own characteristics and should be applied according to the different requirements.

Since the non-overlapping (NOLP) fractional slot windings were proposed for permanent magnet (PM) machines [12], the investigation of dual 3-phase electrical machines with this kind of winding is increasingly popular [13]-[16]. In [13], a specific dual 3-phase electrical machine with 12-slots/10-poles (12S/10P) was fully investigated in terms of the torque performance. The faulty operation with only one set of winding operation was further analyzed and the fault-tolerant capability was identified in [14]. From a more general point of view, the available slot/pole number combinations for constructing dual 3-phase windings were summarized in [15], which provides a quite clear guidance. Authors in [16] emphasized the benefit of harmonic reduction by using Thirty Type dual 3-phase NOLP fractional-slot windings. Since the electrical machines with such kind of winding are inherently semi twelve phase ones, more phase number gives rise to less harmonics and better torque performance. Although a specific PM machine was analyzed, the conclusion is generic. When the phase shift between two sets of windings is different from thirty and zero degrees, more possible configurations can be proposed, as the one shown in [17]-[18]. Moreover, if the suitable harmonic currents are injected into dual 3-phase windings, the torque performance will be improved because of the more flexible current waveform selection [19]-[20].

Y. X. Li, Z. Q. Zhu, and X. M. Wu are with the Electrical Machines and Drives Group, University of Sheffield, Sheffield S1 4DE, U,K, (email: yanxin.li@sheffield.ac.uk; z.q.zhu@sheffield.ac.uk; xwu46@sheffield.ac.uk).

A. S. Thomas, and Z. Y. Wu are with Sheffield Siemens Wind Power Research Centre, North Campus, Sheffield S3 7HQ, U.K. (email: arwyn.thomas@siemensgamesa.com; zhan-yuan.wu@siemensgamesa.com).

When it comes to wind power generation, large size direct-drive low speed PM machines have been widely applied [21]-[22]. Usually, these PM machines adopt either Thirty or Zero Type dual 3-phase modular OLP windings because of the merits mentioned above. Thus, they have larger torque density and higher efficiency compared with doubly-fed induction generators [23]. However, the long stator end winding due to OLP winding and large torque ripple are still troublesome. In order to cope with these issues, NOLP winding may be employed. As has been stated above, the NOLP windings can satisfy the requirement of wind power generators in terms of reducing the end winding and torque ripple. However, the losses could be higher and the efficiency may be reduced if special care is not taken [24]. Furthermore, the stator cores of large size electrical machines cannot be manufactured as the small size ones due to the mechanical restrict on thin laminations. Modularity is always necessary, whereas the conventional all teeth wound NOLP windings will leave the coil sides at the end part of each segment exposed to the air. This increases the potential of winding insulation failure to a large extent during the stator segment transportation and assembly process. Based on this point and enlightened by the idea in [25], the modular machines with NOLP windings and redundant teeth for modularity are proposed.

For more in-depth understanding, this paper extends the analysis of Thirty Type dual 3-phase modular electrical machines with OLP/NOLP windings in [26]. Two specific slot/pole number combinations are chosen as examples to better explain the differences on machine performance. The phase shift is 30 degrees between two sets of windings for both electrical machines and the end parts of stator segments are made of unwound teeth. With the help of finite element analysis (FEA), the electromagnetic performances are compared and the analyses are validated by the experiments.

II. Prototype Machines

The two prototype machines to be comparatively analyzed in this paper have the same rotor pole number, while the stator numbers are different to allow the accommodation of OLP/NOLP windings. The cross-sections are shown in Fig. 1.

From Fig. 1, it can be seen that the modular machines with OLP/NOLP windings have 42-slots/32-poles (42S/32P) and 192S/32P combinations, respectively. Both of their stators can be cut into segments in tooth center, thus the coil sides located at the end parts of each segment can be effectively protected during transportation and assembly process. This is one of the major advantages for the proposed modular machine with NOLP winding. Moreover, the PMs with simple arc shape, viz. without utilizing shaping technique, are adopted for both modular machines to make the comparison easier. It can be foreseen that the modular machine with OLP winding will have much larger torque ripple with such kind of PMs due to quite large cogging torque, which is the major drawback for this kind of PM machine. On the contrary, the modular machine with NOLP winding inherently has quite small cogging torque in usual. For the stator part, the maximal stator segment number is different for two electrical machines (6 and 16 for the 42S/32P and 192S/32P modular machines, respectively), as shown in Fig. 1.

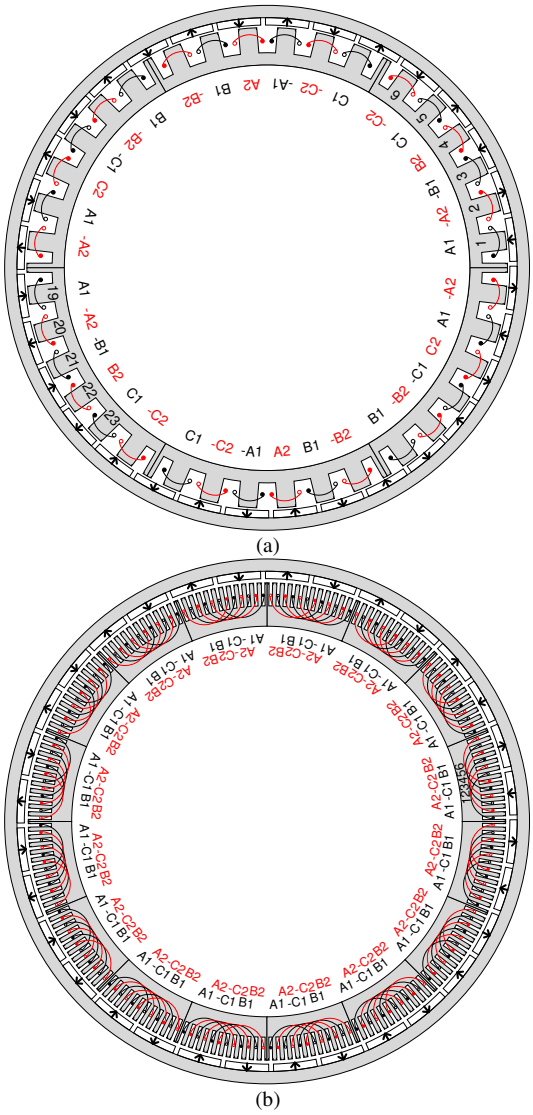

Fig. 1. Cross-sections of two prototype machines. (a) NOLP winding (42S/32P-6 stator segments). (b) OLP winding (192S/32P-16 stator segments).

Besides the stator core structures, the winding layouts of two machines are quite different and should be paid more attention. The star of slots method is used to arrange 36 and 96 winding coils for two modular machines, as shown in Fig. 2.

Fig. 2(a) shows that the phase shifts between adjacent coil EMF vectors within each segment (α_e) are 150 and 30 degrees for two modular machines, respectively. The phase shift between two adjacent end coils (α_r) is the same for two electrical machines, viz. 210 degrees. Three phases within one set of winding have 120 degrees shift between each other (α_{ph}) and two sets of windings differ 30 degrees in space (α_{set}). However, the winding set 2 is 30 degrees ahead referring to the winding set 1 for the 42S/32P modular machine and vice versa for the 192S/32P one, as shown in Fig. 2(b). The minus symbol before the coil number means the wound direction is inward. Although the coil numbers are different for two electrical machines, the turns per phase and rated current are kept the

same to guarantee the similar armature excitation.

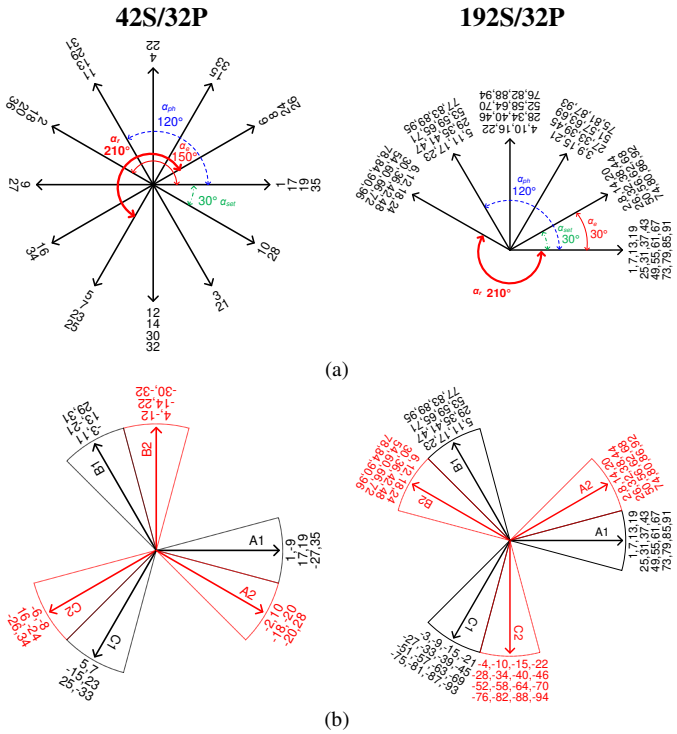

Fig. 2. Windings of two modular machines. (a) Coil electromotive force (EMF) vectors. (b) Winding arrangements.

Before the detailed analysis of the two electrical machines, there are some limitations on structures for the sake of reasonable comparison. Both modular machines have the same stator inner diameter, stator outer diameter, effective slot area, air-gap length, PM thickness, rotor yoke thickness and axial length. The major parameters are listed in TABLE I.

TABLE I. MAJOR STRUCTURE PARAMETERS

Item	Slot number/Pole number	
	42S/32P	192S/32P
Stator inner diameter (mm)	319.4	
Stator outer diameter (mm)	390.4	
Stator yoke thickness (mm)	13.2	16.6
Stator tooth width (mm)	17.52[a] and 7.9[b]	2.98
Air-gap length (mm)	2	
PM thickness (mm)	6	
PM pole arc to pole pitch ratio	0.9	
PM remanence (T)	1.24	
Relative permeability	1.02	
Rotor yoke thickness (mm)	10	
Axial length (mm)	110	
Turns per phase	408	
Phase resistance (Ω)	3.32	4.42
Rated current (A)	3	
Rated speed (rpm)	170	

[a] the teeth with coils.
[b] the teeth without coils.

III. ELECTROMAGNETIC PERFORMANCE COMPARISON

A. *Field Distribution*

When the rotor *d*-axes of two electrical machines coincide with the phase-A1 winding positive direction, the open-circuit flux line distributions at this position are shown in Fig. 3, while the corresponding air-gap flux densities are also compared.

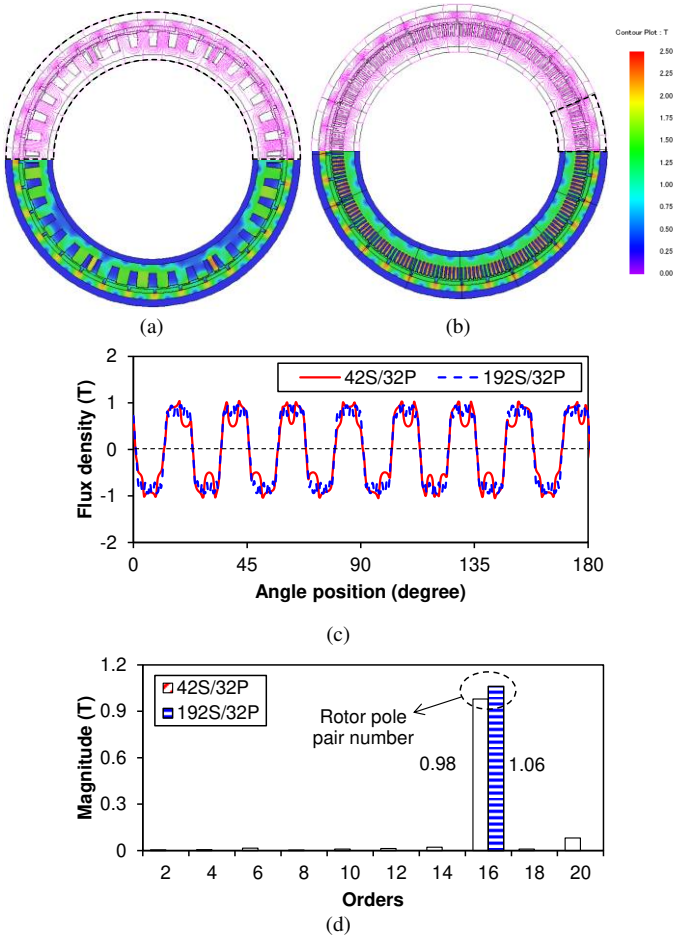

Fig. 3. Open-circuit PM field distributions. (a) Flux line distribution of the 42S/32P modular machine. (b) Flux line distribution of the 192S/32P modular machine. (c) Air-gap flux density waveforms. (d) Air-gap flux density spectra.

In Fig. 3(a) and (b), the minimal repetition unit is highlighted with the dashed lines. There are 2 and 16 repetition units for the 42S/32P and the 192S/32P modular machines, respectively. Since the minimal repetition unit is lower than the rotor pole pair number, the 42S/32P modular machine possesses fractional slot winding which contains much more abundant harmonics than the 192S/32P modular machine whose winding is integer slot type. According to [27], the harmonics for open-circuit field are $2|8n\pm21k|$ and $16|n\pm12k|$ (n=1,3,5… and k=0,1,2…) for the 42S/32P and 192S/32P machines, respectively. From this point of view, the 192S/32P modular machine should have better performance. However, the saturation is severer for this machine as well. Fig. 3(b) implies that quite a few number of stator teeth will be more saturated for the 192S/32P modular machine compared with the 42S/32P one. The redundant teeth of the 42S/32P modular machine are more saturated than effective teeth within each segment due to their narrow width and their influence on machine performance will be seen in the following part. Fig. 3(c) shows that the two electrical machines have non-sinusoidal waveforms but similar peak values in air-gap flux density. In order to clearly see the influence of slot opening, Fig. 3(d) compares their spectra. There is only one working harmonic component, viz. rotor pole pair number, for the 192S/32P modular machine within 20

orders. In contrast, all of the even order harmonics exist in the 42S/32P machine. Due to the larger slot openings in the 42S/32P modular machine, its equivalent air-gap length will be larger and the corresponding working harmonic magnitude will be lower than that of the 192S/32P one.

If two sets of windings are fed with rated current having 30 degree phase shift, the electrical machine runs under rated condition. Since the difference of winding layouts affects the armature field which determines the on-load performance, the armature field distributions with rated current only are shown in Fig. 4. The air-gap flux densities are also given and the results are obtained at the same time instant as the open-circuit situation.

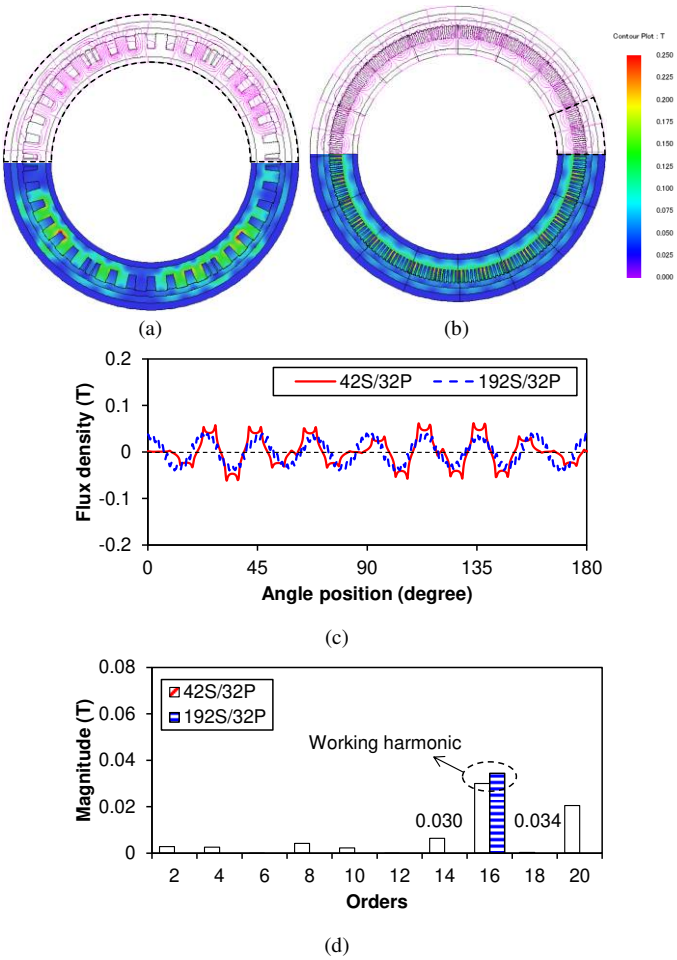

Fig. 4. Field distributions due to armature current only. (a) Flux line distribution of the 42S/32P modular machine. (b) Flux line distribution of the 192S/32P modular machine. (c) Air-gap flux density waveforms. (d) Air-gap flux density spectra.

Since the current of two machines are relatively low, the armature field shown in Fig. 4 is much weaker compared with the PM field shown in Fig. 3. However, the repetition units of armature field are still the same as the PM field. Comparing these two figures, it can also be found that the saturation under armature field only condition is much lower than that under PM field only situation. Thus, the saturation of two electrical machines is still mainly determined by the PM field under rated operation. Fig. 4(c) shows that the armature field waveform of the 42S/32P modular machine is far from the sinusoidal shape in working harmonic order. This is owing to the adoption of fractional slot dual 3-phase winding. The 192S/32P modular machine still keeps 16 repetition units, which is the specialty of integer slot winding. According to [27], the harmonic orders due to armature field are $2|1\pm3k|$ and $16|1\pm12k|$ (k=0,1,2…) for the 42S/32P and 192S/32P modular machines, respectively. From the detailed spectra shown in Fig. 4(d) and above equations, the existence of more harmonics in the 42S/32P modular machine verifies the distortion of its waveform. In contrast, the 192S/32P modular machine has only one component with the same order as the rotor pole pair number. Besides, its magnitude is also higher than that of the 42S/32P one, which is due to smaller slot opening and higher winding factor (0.9659 and 1 for the 42S/32P and 192S/32P modular machines, respectively).

B. Open-circuit back-EMF and cogging torque

When the rotors of two machines rotate under open-circuit condition, the back electromotive force (back-EMF) will be induced in windings and the cogging torque will also be generated. Since the three phases within each set of winding are balanced, only phase-A1 and A2 are chosen as representatives. Their phase back-EMFs are shown in Fig. 5.

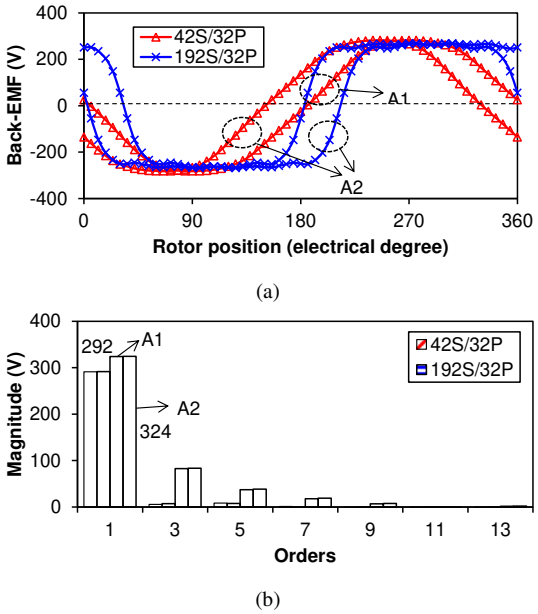

Fig. 5. Open-circuit phase back-EMFs (170 rpm). (a) Waveforms. (b) Spectra.

According to the waveforms shown in Fig. 5(a), the only difference between phase-A1 and A2 back-EMFs is the phase shift direction. Phase-A1 is 30 electrical degrees lag compared with phase-A2 in time for the 42S/32P modular machine and vice versa for the 192S/32P one. This coincides with the phase shift shown in Fig. 2 though the phase shift exhibits in space. Comparing the waveforms of two machines, the 192S/32P modular machine has more trapezoidal back-EMF, which can be more clearly observed in Fig. 5(b). Since all of the harmonics have the same magnitude for phase-A1 and A2, this again verifies that two sets of windings are balanced. The higher fundamental component of the 192S/32P modular machine will contribute to a higher average torque under

on-load condition if the saturation is not heavy. The reason for more sinusoidal back-EMF in the 42S/32P modular machine is due to lower harmonics.

Because of the fully open slots, the non-uniformed air-gap permeance results in the variation of the machine stored energy, which generates cogging torque under open-circuit condition. The results of two electrical machines over one electrical period are shown in Fig. 6.

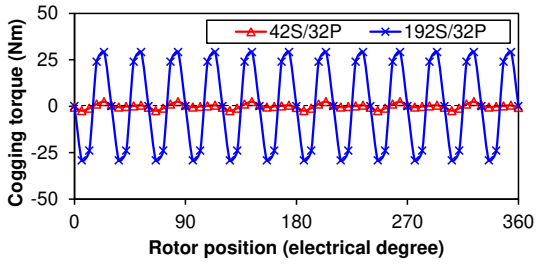

(a)

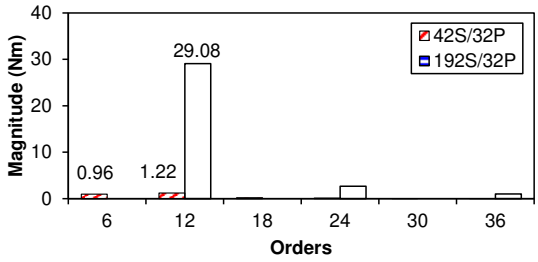

(b)

Fig. 6. Cogging torque. (a) Waveforms. (b) Spectra.

It is quite clear that the modular machine with OLP winding has much larger cogging torque compared with the proposed modular machine with NOLP winding. Fig. 6(a) shows that the 12th harmonic component is predominant in the modular machine with OLP winding, while the lowest cogging torque period number is 6 for the proposed modular machine with NOLP winding. Based on the spectra in Fig. 6(b), the differences between two machines can be more obviously observed. Fig. 6(b) also shows that both 6th and 12th harmonic components exist in the 42S/32P modular machine although they are quite small. Because of the different machine topologies, the minimal cogging torque period over one electrical period (N_{cogpp}) can be obtained as follows:

$$N_{cogpp} = \begin{cases} LCM(N_{trNOLP}, 2p)/p, & for\ NOLP\ windings \\ LCM(N_{sOLP}, 2p)/p, & for\ OLP\ windings \end{cases} \quad (1)$$

where *LCM* means the least common multiple of two numbers; N_{trNOLP} is the redundant tooth number of the proposed modular machines with NOLP windings; p is the rotor pole pair number and N_{sLOP} is the stator slot number of the conventional modular machines with OLP windings. For the two electrical machines analyzed here, N_{cogpp} is 6 and 12, respectively. This is the same as the results shown in Fig. 6.

C. On-load torque

The average torque will be generated when two sets of winding are fed with currents, as shown in Fig. 7. Since there are negligible magnetic reluctance differences between *d*-and *q*-axis, I_d=0 (I_d is *d*-axis current) control strategy is used. As expected, the average torque of the 192S/32P modular machine is higher than that of the 42S/32P one, which is the same as the magnitude of phase back-EMF fundamental component. The torque fluctuation under rated condition shown in Fig. 7(a) seems quite similar to cogging torque and the corresponding spectra shown in Fig. 7(b) can more clearly demonstrate this. The zeroth component represents the average torque and the other harmonic orders are the same as the cogging torque. However, the magnitudes of harmonics have changed, although the increase of magnitude is small. This can be explained by the PM and armature field flux density distributions in Fig. 3 and 4, where the armature field is much weaker than the PM field. That is why the armature field has such negligible influence on torque ripple under rated condition. Since the armature field is related with the current value, the influence of armature field on torque ripple can be seen when the current is high enough.

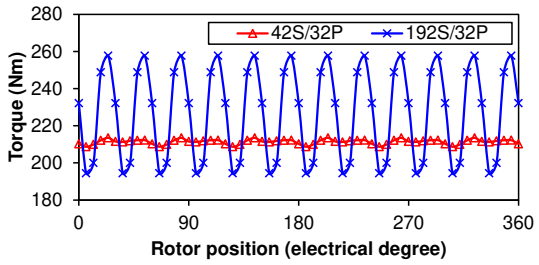

(a)

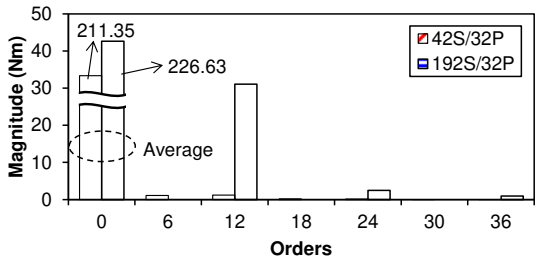

(b)

Fig. 7. On-load torque under rated condition. (a) Waveforms. (b) Spectra.

The complete average and peak-to-peak (PP) torque ripple-current characteristics are shown in Fig. 8. In order to clearly see the influence of armature field on performance, the maximal current is increased up to 15 times of the rated value. Inputting such high current into windings is unrealistic for the real situation and it is only applicable in simulation. Such impractical value is used here only for exaggerating the phenomena for better investigation. It shows that the average torques of both machines gradually increase with the current and show the saturation trend. Although the average torques of two machines are quite close in Fig. 8(a), gradually reduced difference between two machines with the increasing current can still be observed. This is owing to the more saturated stator for the 192S/32P modular machine with higher current. It is the thinner stator teeth that contribute to this. For PP torque ripple, the overall trend is the increase, while the fluctuations can also be observed, especially for the 192S/32P modular machine. The PP torque ripple mainly consists of two components. One

is due to the interaction between PMs and slots and the other is from armature reaction. With the increase of current, these two different components could enhance or weaken each other because of the variation of saturation level. Thus, the PP torque ripple will show the fluctuation. Since the saturation of the 192S/32P modular machine is more sensitive than that of the 42S/32P one, the PP torque fluctuation is more obvious for this electrical machine. No matter the current is low or high, the PP torque ripple is always lower for the 42S/32P modular machine, as shown in Fig. 8(b). This is one of the most important merits for NOLP windings.

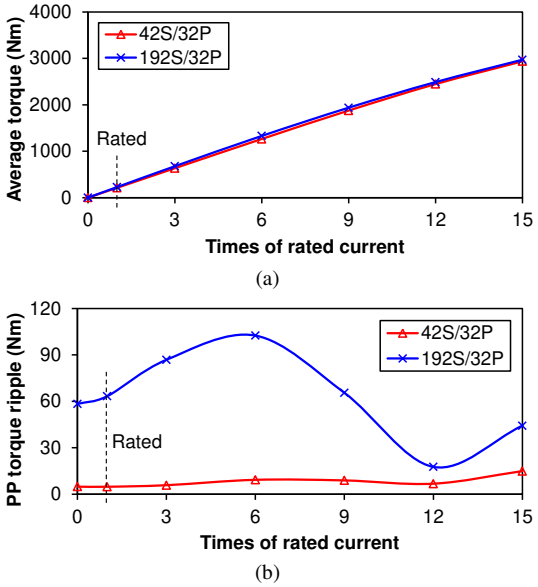

Fig. 8. Influence of current on torque performance. (a) Average torque. (b) PP torque ripple.

D. *Losses and Efficiency*

Due to the change of electrical machine topology, the losses of two electrical machines will show different performances. Laminated stator core iron loss (P_{Fe}), solid PM and solid rotor yoke eddy current losses (P_{PM} and P_{ry}, respectively) are three major losses components to be concerned. They can be predicted based on the following equations in the post process of FEA:

$$\begin{aligned} P_{Fe} &= k_h B_m^{\alpha} f + k_e B_m^2 f^2 \\ \alpha &= K_{f1} f^2 + K_{f2} f + K_{f3} \end{aligned} \tag{2}$$

$$P_{PM} = \frac{\omega_e}{2\pi} \int_0^{\frac{2\pi}{\omega_e}} \left(\sum_{i=1}^{N_p} \iint_{S_{PMi}} [J_{PMi}^2(t) / \sigma_{PM}] ds \right) dt \tag{3}$$

$$P_{ry} = \frac{\omega_e}{2\pi} \int_0^{\frac{2\pi}{\omega_e}} \left(\iint_{S_{ry}} [J_{ry}^2(t) / \sigma_{ry}] ds \right) dt \tag{4}$$

where k_h and k_e are the hysteresis and eddy current loss coefficients of stator lamination; B_m is the magnitude of flux density; f is the frequency; K_{f1}, K_{f2} and K_{f3} are determined by the material property; ω_e is the angular frequency in rad/s; S_{PMi} and S_{ry} are the area of the i^{th} PM and rotor yoke; J_{PMi} and J_{ry} are the current density of the i^{th} PM and rotor yok; σ_{PM} and σ_{ry} (740000 and 6000000 S/m for PMs and rotor cores of the machines in this paper) are the rotor yoke conductivity of PM and rotor yoke. Since all of them are also closely related to the armature field, the variations of these losses with current are shown in Fig. 9. Again, the current is increased to unrealistic 15 times of the rated value for clearer demonstration.

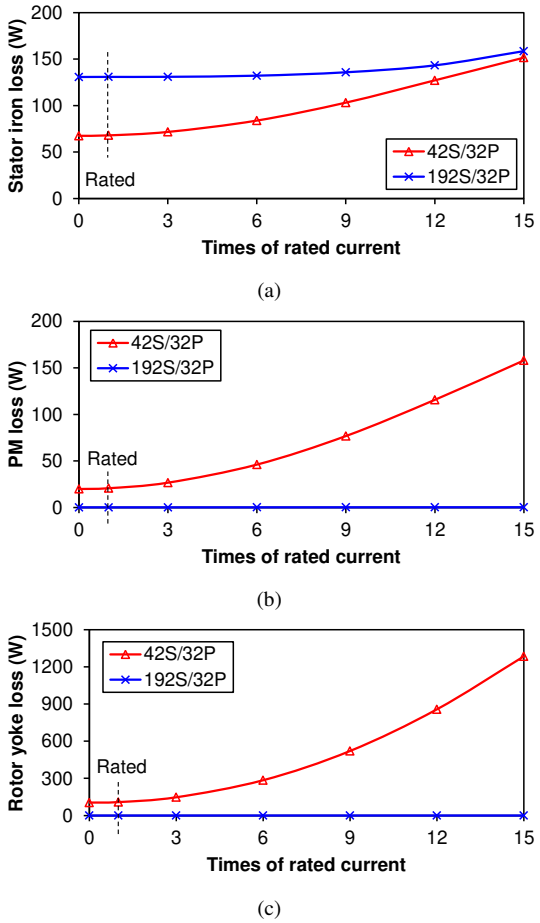

Fig. 9. Variation of losses with the current (170 rpm). (a) Stator iron loss. (b) PM eddy current loss. (c) Rotor yoke eddy current loss.

Fig. 9(a) shows that the dual 3-phase modular machine with NOLP winding has lower stator iron loss compared with the one with OLP winding. This comes from the lower stator core saturation, although the difference between two machines will increasingly low with the increase of current. Fig. 9(b) and (c) demonstrate that the other two kinds of losses are almost negligible for the 192S/32P machine compared with the relative huge value for the 42S/32P one. As it can be clearly observed in Fig. 3 and 4, the harmonics are really more abundant for the 42S/32P modular machine no matter for the PM or armature field. Because of extremely low harmonic contents, the PM and rotor yoke eddy current losses are pretty small for the dual 3-phase machine with OLP winding, even if the current is high. However, the difference of two loss components can be found in the 42S/32P modular machine. Since the PMs are separated with each other, some lower order harmonics having longer wavelength will be suppressed. For the rotor yoke, there are no interruptions in the yoke body; and therefore all of the harmonics except the synchronous one will generate eddy current loss. That is why this component will be larger than the PM eddy current loss and the difference will

become larger and larger with the increase of current. For the real applications, other measures must be adopted to reduce these two losses. It should be mentioned that the skin effect of flux density with high frequency variation is hard to be accurately considered; therefore the accuracy of the eddy current loss for integer slot machine needs more mesh elements. The step number must be high enough to account for higher order harmonics, especially for the high speed operations.

Besides these three iron loss components, the stator copper loss (P_{cop}) is one of the major losses in PM machines, which can be predicted by:

$$P_{cop} = mI_{ph}^2 R_{ph} \tag{5}$$

where m is the phase number; I_{ph} is the phase current in root mean square (RMS) value and R_{ph} is the phase resistance. For the two machines analyzed in this paper, the phase resistances are shown in TABLE I. Thus, the corresponding copper losses are obtained.

For other losses, such as mechanical friction loss, winding loss, etc., they are much less than above four types of losses and are not considered for simplicity. Finally, the efficiency (η) can be calculated by:

$$\eta = (P_{em} - P_{PM} - P_{ry})/(P_{em} + P_{Fe} + P_{cop}) \times 100\%$$
$$P_{em} = T_{em}\Omega_r \tag{6}$$

where P_{em} and T_{em} are the electromagnetic power and torque, respectively; $.\Omega_r$ is the rotor mechanical speed in rad/s. The calculation results are listed in TABLE II for rated condition.

TABLE II. LOSSES AND EFFICIENCY

Item	Slot number/Pole number	
	42S/32P	192S/32P
Stator copper loss (W)	179.28	238.68
Stator iron loss (W)	67.91	130.82
PM eddy current loss (W)	20.68	0.13
Rotor yoke eddy current loss (W)	108.43	0.06
Electromagnetic power (W)	3762.35	4035.79
Efficiency (%)	90.61	91.61

It shows that the proposed modular machine with NOLP winding has lower copper loss and stator iron loss, while the modular machine with OLP winding has negligible PM and rotor yoke losses. The reason for these differences has been illustrated above, and the efficiencies of both machines are similar. From TABLE II, it can be seen that these two modular machines do not have very high efficiency which should be achieved for the PM machines in this size. The dimensional constraints given by the customer are the major reasons. On one hand, the air-gap, viz. 2mm, is too large for these two machines, which will reduce the machine performance and increase the losses. On the other hand, the stator core is not fully utilized due to the restriction on the slot area, which leads to the use of very thin wire for the winding and large copper loss is generated.

E. Inductance characteristic

Since two prototype machines have different winding topologies, the corresponding inductances will show different characteristics as well. Phase inductances can show the coupling between different phases, which is the criteria to judge the mutual influence under faulty conditions. For *d*- and *q*-axis inductances, they can reflect the saliency and the short-circuit fault withstand capability. The frozen permeability method is used to predict these inductances [28]:

$$L_{ij} = \psi_{ij(F)}/I_j$$
$$i, j = A1,\ A2,\ B1,\ B2,\ C1,\ C2\ or\ d-\ and\ q-axis \tag{7}$$

where L_{ij} represents the inductance between i and j; $\psi_{ij(F)}$ is the flux linkage obtained under the specific operation condition by frozen permeability method. I_j is the current used to calculate the inductance. The inductance waveforms are shown in Fig. 10 and the average values are summarized in TABLE III.

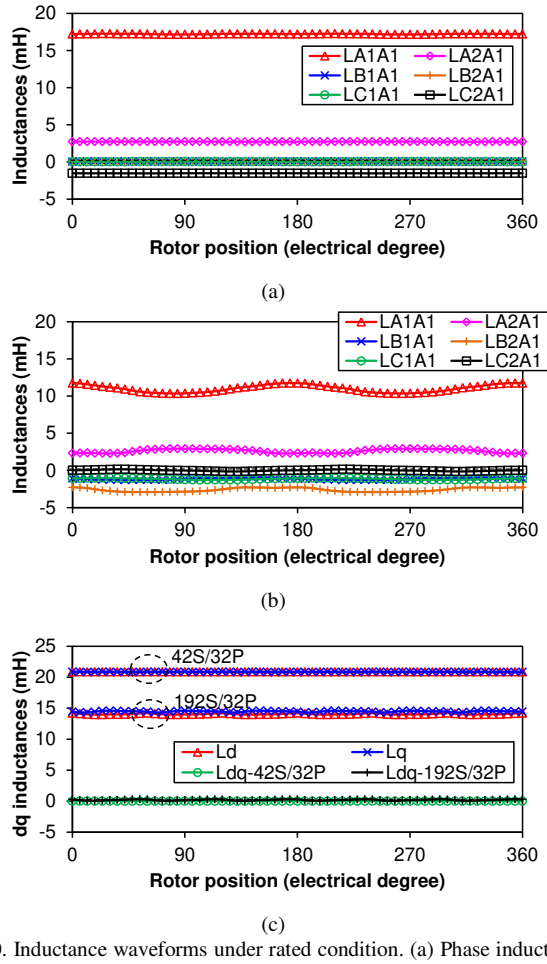

Fig. 10. Inductance waveforms under rated condition. (a) Phase inductance of 42S/32P modular machine. (b) Phase inductance of 192S/32P modular machine. (c) *d*- and *q*-axis inductances.

TABLE III. INDUCTANCES

Item	Slot number/Pole number	
	42S/32P	192S/32P
L_{A1A1} ($\lvert L_{A1A1}/L_{A1A1}\rvert$ x 100%)	17.2147 (100%)	11.0144 (100%)
L_{B1A1} ($\lvert L_{B1A1}/L_{A1A1}\rvert$ x 100%)	0.0411 (2.39%)	-1.1506 (10.45%)
L_{C1A1} ($\lvert L_{C1A1}/L_{A1A1}\rvert$ x 100%)	0.0411 (2.39%)	-1.1502 (10.44%)
L_{A2A1} ($\lvert L_{A2A1}/L_{A1A1}\rvert$ x 100%)	2.7338 (15.88%)	2.6093 (23.69%)
L_{B2A1} ($\lvert L_{B2A1}/L_{A1A1}\rvert$ x 100%)	0.1164 (6.76%)	-2.6090 (23.69%)
L_{C2A1} ($\lvert L_{C2A1}/L_{A1A1}\rvert$ x 100%)	-1.5252 (8.86%)	0.0003 (0.00%)
L_d	20.8778	14.0492
L_q	20.8478	14.4702
L_{dq}	-0.0070	0.1828

From Fig. 10 and TABLE III, it can be seen that the mutual phase coupling is more evident for the 192S/32P modular machine due to the adoption of OLP winding. Furthermore, the overlapped end windings will more obviously affect other phases under faulty conditions. The negligible difference between *d*- and *q*-axis inductances shows that there is no reluctance torque for both machines. The larger *d*-axis inductance is better for impede the short-circuit current. This is another advantage for the proposed modular machine with NOLP winding.

IV. Experimental Validation

The proposed 42S/32P modular machine with redundant teeth has been prototyped to validate the analyses in this paper. The photo of this electrical machine and the corresponding test rig are shown in Fig. 11. In Fig. 11(a), the air-gap of the prototype is maintained by a single-sided bearing at the back and its front part of the stator is fixed with the shaft via the end plate. The shaft center leaves the space for the torque transducer and the shaft front part supporter. Several thermocouples are inserted into the slot for the future thermal study. PMs are stick to the rotor yoke which is made of solid steel. A zoomed view of the stator core segment connection part is shown in Fig. 11(b). It can be seen that stator segments are fixed together by the end plate as well and there is an additional air-gap between adjacent stator core segments. This assembly tolerance is unavoidable and its value is found to be about 1mm in this prototyped machine. The side effect of this additional air-gap will be observed in the following results. Fig. 11(c) shows the complete test platform with the installed prototype machine. The dynamometer is a direct current (DC) machine and it can be supplied by the DC source. The control cabinet integrates the converters and their controllers and protects the prototype machine.

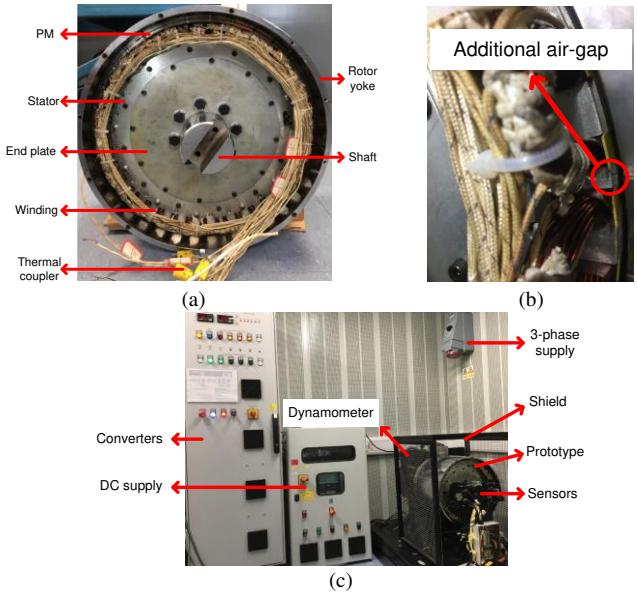

Fig. 11. Experimental facilities. (a) Prototyped modular machine. (b) Zoomed view for the additional air-gap between adjacent segments. (c) Test rig.

The measured open-circuit back-EMFs of phase-A1 and -A2 are compared in Figs. 12(a) and (b) at the rated speed. It shows that both waveforms and spectra match quite well with the FEA predicted results. The matched back-EMFs demonstrate that the winding connections of the prototype machine are correct. The open-circuit cogging torque is also measured and the results are plotted in Figs. 12(c) and (d).

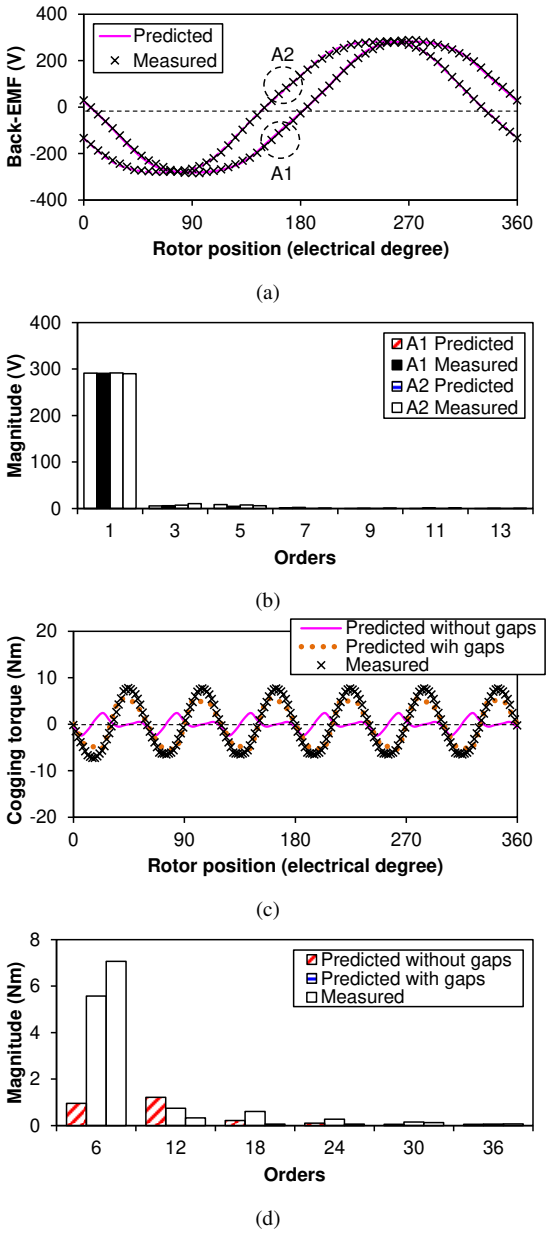

Fig. 12. Comparison of predicted and measured back-EMF and cogging torque. (a) Back-EMF waveforms (170 rpm). (b) Back-EMF harmonics. (c) Cogging torque waveforms. (d) Cogging torque spectra.

It can be seen that the differences between measured and ideal FE predicted results are significant. It is found that the additional air-gaps between six stator segments are the reason for such difference. As shown in Fig. 11(b), the influence of 1mm additional gap between segments should be taken into account for the accurate performance prediction. Fig. 12(c) and (d) validate that the good agreement can be seen between prediction and measurement when manufacture tolerances are considered. It must be acknowledged that 1mm additional

air-gap length is a bit large for this prototype machine, since the mechanical air-gap length is just 2mm. The reason for such large manufacture tolerance is owing to the lack of experience in producing such kind of PM machine. Although there are some side effects causing by this manufacture tolerance, the efficacy of the analysis is still trustworthy.

The on-load torque and torque-current characteristic again match well between the predicted and measured results, as shown in Fig. 13. Fig. 13(a) and (b) show that the difference between the measured torque waveform and the ideal FE result arises from the additional air-gap side effect as well. A bit lower average torque should be the consequence of axial end leakage effect. Because of the additional air-gaps, the equivalent air-gap length will be larger, which reduces the predicted average torque. The almost linear variation of on-load torque with current in Fig. 13(c) verifies that the armature reaction is not strong enough to make the prototype machine very saturated.

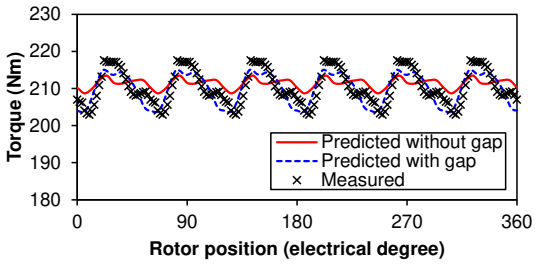

(a)

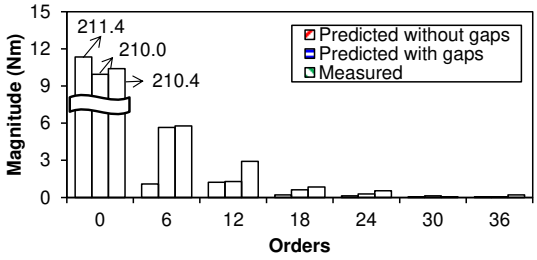

(b)

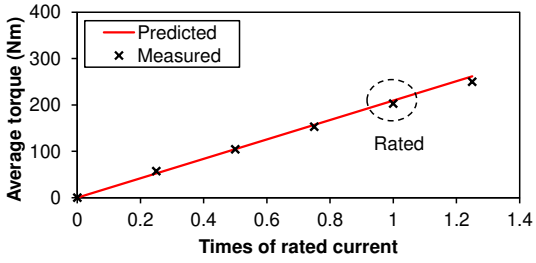

(c)

Fig. 13. Comparison of predicted and measured torques. (a) Waveforms (170rpm). (b) Harmonics. (c) Torque-current characteristics.

Before measuring the efficiency-speed characteristic, the corresponding torque-speed characteristic is firstly identified. Then the efficiency-speed characteristic can be obtained from those sample points on the torque-speed curve. Both half load and full load situations are considered and compared in Fig. 14. Since the prototyped modular machine is surface-mounted PM type and is used for low speed direct drive situations, the flux-weakening capability is limited and usually not required, as shown in Fig. 14(a). For those measured efficiencies, relative larger errors can be seen in Fig. 14(b), because the additional losses due to manufacture tolerances and the mechanical friction are not included in predictions. The reason for not high efficiency is the unreasonable dimension restricts as previously explained.

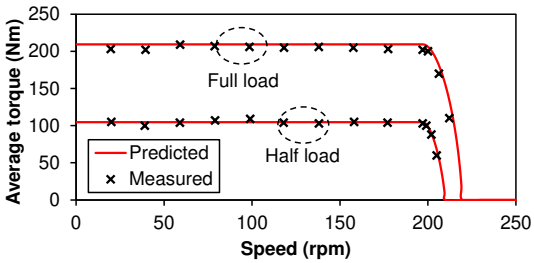

(a)

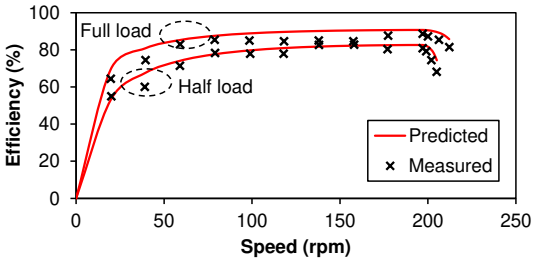

(b)

Fig. 14. Comparison of predicted and measured torque and efficiency vs speed. (a) Torque-speed characteristics. (b) Efficiency-speed characteristics.

The measured phase inductances are compared with the predicted ones, as shown in TABLE IV. The relative difference (RD), viz. (1-Measured/Predicted) x 100%, is used to show the difference. For the self-inductance, the RD is lower due its larger value compared with the mutual inductances. Some mutual inductances are too small to be accurately measured, which shows a larger RD in TABLE IV.

Overall, the experimental results can validate the efficacy of the analyses in this paper.

TABLE IV. COMPARISON OF MEASURED AND PREDICTED INDUCTANCES

Item	Predicted	Measured	RD(%)	Item	Predicted	Measured	RD(%)
L_{A1A1}	17.2147	17.8511	3.7	L_{A2A1}	2.7338	2.3522	14.0
L_{B1A1}	0.0411	0.0535	30.2	L_{B2A1}	0.1164	0.1300	11.7
L_{C1A1}	0.0411	0.0512	24.6	L_{C2A1}	-1.5252	-1.3325	12.6

V. CONCLUSION

This paper presents two specific modular machines with different stator topologies but the same major dimensions to show the differences by using OLP and NOLP windings. A 42S/32P modular dual 3-phase PM machine with NOLP winding and redundant teeth for easy modularity has been proposed for wind power generation. It is compared with a conventional 192S/32P one having OLP winding. The analyses show that the proposed 42S/32P modular machine has comparable electromagnetic performance in terms of average torque and efficiency. The PP torque ripple of the 192S/32P machine with OLP winding is always much larger compared with the one with NOLP winding regardless of the current value. When it comes to the fault-tolerant capability, the

42S/32P modular machine has much weaker mutual coupling between different phases and the larger *d*-axis inductance which is beneficial to reducing short-circuit current. Besides these merits, the proposed modular PM machines with NOLP windings will generate larger PM and rotor yoke eddy current losses, which reduces the machine efficiency and increases the potential thermal demagnetization. This must be considered for the real applications. For clarity, the pros and cons by using OLP and NOLP windings in modular PM machines are summarized in TABLE V, together with the reasons.

TABLE V. PROS AND CONS OF OLP AND NOLP WINDINGS

Item	OLP windings	NOLP windings	Reasons
Average torque	A bit larger	A bit smaller	(1) Larger winding factors for OLP windings; (2) Smaller slot openings for modular machines with OLP windings.
Torque ripple	Much larger	Much smaller	(1) Lower cogging torque for modular machines with NOLP windings; (2) Lower saturation for the stators with NOLP windings.
End winding length	Much longer	Much shorter	Slot pitch is only one for NOLP windings.
Efficiency	Similar		Lower copper loss and stator iron loss but higher rotor loss for modular machines with NOLP windings.
Fault-tolerance	Lower	Higher	Lower mutual inductances among phases and higher *d*-axis inductance for NOLP windings;
Manufacturability	More complex	Simpler	(1) Fewer stator segments for modular machines with NOLP windings; (2) Lower volume for modular machines with NOLP windings. (3) Simple coil shape for NOLP windings.

Beyond the discussion in this paper, several tasks could be the future work, such as faulty operation with the failure segment, unbalanced voltage caused by different end winding leakage inductance and vibration characteristics. In summary, both modular machines have their own merits and demerits. Although two specific modular machines are analyzed, the conclusions could be effective to other modular machines with different slot and pole number combinations.

ACKNOWLEDGMENT

This work is supported by the UK EPSRC Prosperity Partnership Project on “A New Partnership in Offshore Wind”, EP/R004900/1.

REFERENCES

[1] E. Levi, “Multiphase electric machines for variable-speed applications,” *IEEE Trans. Ind. Electron.*, vol. 55, no. 5, pp. 1893-1909, May 2008.

[2] A. M. El-Refaie, “Fault-tolerant permanent magnet machines: a review,” *IET Proc. -Electr. Power Appl.*, vol. 5, no. 1, pp. 59-74, Jan. 2011.

[3] E. F. Fuchs, and L. T. Rosenberg, “Analysis of an alternator with two displaced stator windings,” *IEEE Trans. Power App. Syst.*, vol. 93, no. 6, pp. 1776-1786, Nov. 1974.

[4] T. M. Jahns, “Improved reliability in solid-state AC drives by means of multiple independent phase drive units,” *IEEE Trans. Ind. Appl.*, vol. IA-16, no. 3, pp. 321-331, May/June 1980.

[5] E. A. Klingshirn, “High phase order induction motors-part I-description and theoretical considerations,” *IEEE Trans. Power App. Syst.*, vol. 102, no. 1, pp. 47-53, Jan. 1983.

[6] M. A. Abbas, R. Christen, and T. M. Jahns, “Six-phase voltage source inverter driven induction motor,” *IEEE Trans. Ind. Appl.*, vol. 16, no. 3, pp. 1251-1259, May/June 1984.

[7] K. Gopakumar, V. T. Ranganthan, and S. R. Bhat, “Split-phase induction motor operation from PWM voltage source inverter,” *IEEE Trans. Ind. Appl.*, vol. 29, no. 5, pp. 927-932, Sept./Oct. 1993.

[8] Y. F. Zhao, and T. A. Lipo, “Space vector PWM control of dual three-phase induction machine using vector space decomposition,” *IEEE Trans. Ind. Appl.*, vol. 31, no. 5, pp. 1100-1109, Sept./Oct. 1995.

[9] D. Hadiouche, H. Razik, and A. Rezzoug, “On the modeling and design of dual-stator windings to minimize circulating harmonic currents for VSI fed AC machines,” *IEEE Trans. Ind. Appl.*, vol. 40, no. 2, pp. 506-515, Mar./Apr. 2004.

[10] D. Hadiouche, L. Baghli, and A. Rezzoug, “Space-vector PWM techniques for dual three-phase AC machine: analysis, performance evaluation, and DSP implementation,” *IEEE Trans. Ind. Appl.*, vol. 42, no. 4, pp. 1112-1122, July/Aug. 2006.

[11] S. Basak, and C. Chakraborty, “Dual stator winding induction machine: problems, progress, and future scope,” *IEEE Trans. Ind. Electron.*, vol. 62, no. 7, pp. 4641-4652, July 2015.

[12] T. Kenjo, and S. Nagamori, *Permanent-magnet and Brushless DC Motors*. Oxford University Press, 1985.

[13] M. Barcaro, N. Bianchi, and F. Magnussen, “Analysis and tests of a dual three-phase 12-slot 10-pole permanent-magnet motor,” *IEEE Trans. Ind. Appl.*, vol. 46, no. 6, pp. 2355-2362, Nov./Dec. 2010.

[14] M. Barcaro, N. Bianchi, and F. Magnussen, “Faulty operations of a PM fractional-slot machine with a dual three-phase winding,” *IEEE Trans. Ind. Electron.*, vol. 58, no. 9, pp. 3825-3832, Sept. 2011.

[15] M. Barcaro, N. Bianchi, and F. Magnussen, “Six-phase supply feasibility using a PM fractional-slot dual winding machine,” *IEEE Trans. Ind. Appl.*, vol. 47, no. 5, pp. 2042-2050, Sep./Oct. 2011.

[16] P. Zheng, F. Wu, Y. Sui, P. F. Wang, Y. Lei, and H. P. Wang, “Harmonic analysis and fault-tolerant capability of a semi-12-phase permanent-magnet synchronous machine used for EVs,” *Energies*, vol. 5, no. 9, pp. 3586-3607, Sep. 2012.

[17] V. I. Patel, J. B. Wang, W. Y. Wang, and X. Chen, “Six-phase fractional-slot-per-pole-per-phase permanent-magnet machines with low space harmonics for electric vehicle application,” *IEEE Trans. Ind. Appl.*, vol. 50, no. 4, pp. 2554-2563, July/Aug. 2014.

[18] P. L. Xu, J. H. Feng, S. Y. Guo, S. Z. Feng, W. Q. Chu, Y. Ren, et al., “Analysis of dual three-phase permanent magnet synchronous machines with different angle displacements,” *IEEE Trans. Ind. Electron.*, vol. 65, no. 3, pp. 1941-1954, Mar. 2018.

[19] K. Wang, Z. Q. Zhu, Y. Ren, and G. Ombach, “Torque improvement of dual three-phase permanent magnet machine with 3rd harmonic current injection,” *IEEE Trans. Ind. Electron.*, vol. 62, no. 11, pp. 6833-4844, Nov. 2015.

[20] Y. S. Hu, Z. Q. Zhu, and M. Odavic, “Torque capability enhancement of dual three-phase PMSM drive with fifth and seventh current harmonics injection,” *IEEE Trans. Ind. Appl.*, vol. 53 , no. 5, pp. 4526-4535, Sept./Oct. 2017.

[21] Y. C. Chen, P. Pillay, and A. Khan, “PM wind generator topologies,” *IEEE Trans. Ind. Appl.*, vol. 41, no. 6, pp. 1619-1626, Nov./Dec.2005.

[22] S. F. Jia, R. H. Qu, J. Li, X. G. Fan, and M. Zhang, “Study of direct-drive permanent-magnet synchronous generators with solid rotor back iron and different windings,” *IEEE Trans. Ind. Appl.*, vol. 52, no. 2, pp. 1369-1379, Mar./Apr. 2016.

[23] J. Y. Chen, C. V. Nayar, and L. Y. Xu, “Design and finite-element analysis of an outer-rotor permanent-magnet generator for directly coupled wind turbines,” *IEEE Trans. Magn.*, vol. 36, no. 5, pp. 3802-3809, Sept. 2000.

[24] M. Cheng, and Y. Zhu, “The state of the art of wind energy conversion systems and technologies: A review,” *Energy Conversion and Management*, vol. 88, pp. 332-347, 2014.

[25] Y. G. Chen, Z. M. Du, W. G. Zhong, and L. B. Kong, “Modular stator structure permanent magnet synchronous machine,” in *World Automation Congress (WAC 2008)*, Sept. 28-Oct.2, 2008, pp. 1-5.

[26] Y. X. Li, Z. Q. Zhu, X. M. Wu, A. S. Thomas, and Z. Y. Wu, “Comparison of modular dual 3-phase PM machines with overlapping/non-overlapping windings,” in *IEEE Energy Conversion Congress and Exposition (ECCE 2018)*, Sept. 23-27, 2018, pp. 2335-2342.

[27] B. Hannon, P. Sergeant, and L. Dupré, “Time- and spatial-harmonic content in synchronous electrical machines,” *IEEE Trans. Magn.*, vol. 53, no. 3, pp. 1-11, Mar. 2017.

[28] J. A. Walker, D. G. Dorrell, and C. Cossar, “Flux-linkage calculation in permanent-magnet motors using the frozen permeabilities method,” *IEEE Trans. Magn.*, vol. 41, no. 10, pp. 3946-3948, Oct. 2005.